Journal of Sound and Vibration (2000) **236**(4), 683–703
doi:10.1006/jsvi.2000.3039, available online at http://www.idealibrary.com on IDEAL®

INTERNAL RESONANCES IN WHIRLING STRINGS INVOLVING LONGITUDINAL DYNAMICS AND MATERIAL NON-LINEARITIES

MICHAEL J. LEAMY* AND ODED GOTTLIEB

Faculty of Mechanical Engineering, The Technion — Israel Institute of Technology, Haifa 32000, *Israel*

(*Received* 8 *November* 1999, *and in the final form* 21 *March* 2000)

Internal resonance mechanisms between near-commensurate longitudinal and transverse modes of a taut spatial string are identified and studied using an asymptotic method, and the influence of material non-linearities on the resulting solutions is considered. Geometrical non-linearities couple longitudinal motions to in-plane and out-of-plane transverse motions, resulting in resonant and non-resonant interactions between linearly orthogonal string modes. Past studies have included only transverse modes in the description of string motions and have predicted periodic, quasi-periodic, and chaotic whirling motions arising from the geometrical non-linearities. This study considers further the inclusion of longitudinal motions and a non-linear material law, which are both appropriate for the study of rubber-like strings. An asymptotic analysis captures the aforementioned whirling motions, as well as a new class of whirling motions with significant longitudinal content. Periodic, quasi-periodic, and aperiodic (likely chaotic) responses are included among these motions. Their existence, hardening–softening characterization, and stability are found to be highly dependent on the magnitude of the material non-linearities.

1. INTRODUCTION

Many studies have examined the non-linear dynamics of spatial strings with *linear* material descriptions and non-resonant longitudinal response. Among these are the study by Narasimha [1], in which a transversely excited model was developed capturing whirling string motions while correctly accounting for non-resonant longitudinal motions. A later study by Miles [2] used an asymptotic theory to develop evolution equations governing the slowly varying modal amplitudes. Using a local bifurcation analysis, the thresholds for periodic and quasi-periodic whirling were predicted, although the existence of chaotic motions was not shown until later when Johnson and Bajaj [3] studied the evolution equations numerically and when Molteno and Tufillaro [4] and O'Reilly and Holmes [5] reported experimental observations of torus doubling and chaotic string motions. Global bifurcation theory was utilized to explain the existence of chaotic attractors numerically by Bajaj and Johnson [6] and analytically by O'Reilly and Holmes [5] and O'Reilly [7]. However, only qualitative agreement has been documented to date between (weakly) non-linear theory and experiments of quasi-periodic or chaotic whirling strings. Numerical simulation of the (strongly) non-linear string by Rubin and Gottlieb [8] revealed that the onset of persistent periodic whirling and aperiodic response is about 5 times smaller than

* Author to whom correspondence should be addressed. NASA Langley Research Center, Mail Stop 201, 11W. Taylor Street, Bldg. 1146, Room 116, Hampton, VA 23601, U.S.A.

0022-460X/00/390683 + 21 $35.00/0

that observed in experiments. Some possible explanations offered for this discrepancy include not consistently modelling aeroelastic drag and boundary dissipation, and not including non-linear material properties.

Nylons [9] and rubber-like materials, including latex [10], can exhibit stress–strain behavior in which linear and non-linear effects are of equal importance. Nayfeh *et al.* [10] examined analytically and experimentally a latex string forced near a transverse natural frequency, without including material non-linearities in their analytical model. They found good agreement between their experimental and analytical results for periodic planar and whirling motions when no parametric excitation of the longitudinal modes occurred, but found discrepancies in the parametrically excited case that they attributed to the presence of longitudinal motions. Furthermore, in parameter regimes where their analytical model predicted modulated motions, they observed only periodic response in their experimental studies. They did not comment on discrepancies that might be present due to not modelling non-linear material properties. Leamy and Gottlieb [11] introduced a new modelling approach for the spatial string, with sufficient generality to include strings composed of non-linear materials, by employing finite deformation continuum mechanics and a non-linear material constitutive law. Analyzing separately transverse and longitudinal motions using asymptotics, they found that the material non-linearities had a negligible effect on transversely dominated string motions, but influenced the degree of non-linearity and the softening–hardening nature of longitudinally dominated string motions.

In this investigation, internal resonances between longitudinal modes and transverse modes will be analyzed for a string described by a non-linear material law. The string model developed in Leamy and Gottlieb [11] is summarized and adapted to study the relevant internal resonance. A convenient non-dimensionalization is introduced and an approximate solution procedure is completed by direct application of the multiple scales method on the three governing partial differential equations. The solutions are interpreted for example strings and the results are used to document periodic, quasi-periodic, and aperiodic (likely chaotic) responses.

2. NON-LINEAR STRING MODEL

The non-linear string model chosen for this study is that developed recently by Leamy and Gottlieb [11], which incorporates a non-linear material constitutive law and finite deformation continuum mechanics. A cursory description of the model is given below before proceeding directly to the governing equations.

A pre-tensioned string with length L, mass-per-unit length $\rho^{\mathrm{T}}A^{\mathrm{T}}$, and initial tension T_0 is considered to deform in three-dimensional space under the influence of general excitation. As depicted in Figure 1, rectilinear material co-ordinates (x_1, x_2, x_3) are chosen to identify material points along the string in the tensioned (initial) configuration, where x_1 is along the length of the string. An inertial co-ordinate system (z_1, z_2, z_3) with unit vectors $(\mathbf{I}_1, \mathbf{I}_2, \mathbf{I}_3)$ is defined which corresponds to the material co-ordinate system in the tensioned configuration. The material co-ordinates are convected with the string's deformation into a triad of non-orthogonal curvilinear co-ordinates (x^1, x^2, x^3), which are used to characterize the deformed state of the string. Similarly, unit vectors $(\mathbf{i}_1, \mathbf{i}_2, \mathbf{i}_3)$ along (x_1, x_2, x_3) in the tensioned configuration are convected into covariant base vectors $(\mathbf{G}_1, \mathbf{G}_2, \mathbf{G}_3)$ along (x^1, x^2, x^3) in the deformed configuration, where it is noted that in general, these base vectors are no longer mutually orthogonal nor have unit length.

Following a formulation of the strain energy, kinetic energy, and external virtual work, application of Hamilton's Principle yields the following field equations and boundary

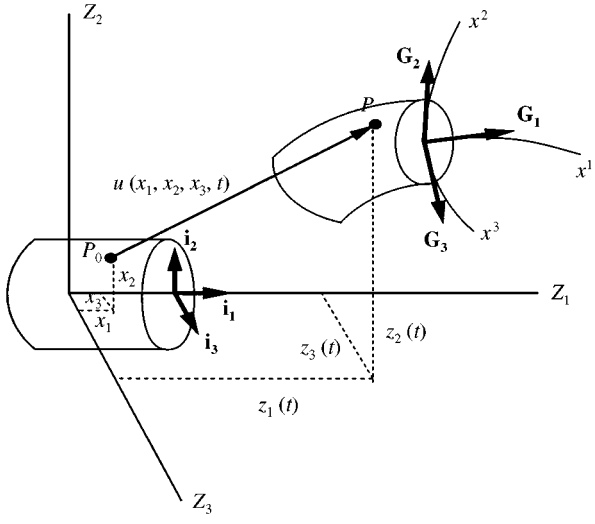

Figure 1. Diagram depicting a small element of the string in both the tensioned and the deformed configuration. Material co-ordinates (x_1, x_2, x_3) identify a point P_0 in the tensioned configuration, which is displaced during deformation to point P and is located in space by the inertial co-ordinates $(z_1(t), z_2(t), z_3(t))$. After deformation, the material co-ordinates form a non-orthogonal curvilinear co-ordinate system (x^1, x^2, x^3) with covariant base vectors $(\mathbf{G}_1, \mathbf{G}_2, \mathbf{G}_3)$.

conditions:

$$(A^{\mathrm{T}} t^{11}(\delta_{1m} + u_{m,1}))_{,1} + \rho^{\mathrm{T}} A^{\mathrm{T}} \hat{F}_m = \rho^{\mathrm{T}} A^{\mathrm{T}} \ddot{u}_m, \tag{1}$$

$$A^{\mathrm{T}} t^{11}(\delta_{1m} + u_{m,1}) \delta u_m \Big|_{x^1 = 0}^{x^1 = L} = 0, \tag{2}$$

where a comma denotes differentiation with respect to the material co-ordinates, the repeated subscript signifies summation, δ_{ij} represents the Kronecker delta, t^{ij} denotes the second Piola–Kirchoff stress tensor representing the stress state per unit area in the *tensioned* configuration referred to the material co-ordinate system, $u_m(x_1, t)$ denotes the displacement field, and $\hat{F}_m$ denotes external forces per unit mass. Specifically, direct excitation at $x_1 = L/2$, viscous drag, and the gravitational body force appear in $\hat{F}_m$ as

$$\hat{F}_m = \frac{\alpha_m P(t)}{\rho^{\mathrm{T}} A^{\mathrm{T}}} \delta(x_1 - L/2) - c_m \dot{u}_m - \beta_m g, \tag{3}$$

where g denotes the gravitational acceleration, $P(t)$ denotes the forcing, $\delta(x - a)$ denotes the Dirac delta generalized function acting at $x = a$, c_m denotes viscous damping coefficients, and α_m and β_m denote direction cosines, of which α_3 and β_3 are chosen to be zero.

For this study, the string is assumed to be simply supported with boundary conditions

$$u_m(0, t) = u_m(L, t) = 0, \quad m = 1, 2, 3, \tag{4}$$

which satisfy equation (2).

Following Oden [12] and Meirovitch [13], the constitutive relationship for an isotropic, viscoelastic (Kelvin–Voigt) material is stated here as

$$t^{ij} = \frac{\partial \mathscr{W}}{\partial \gamma_{ij}} + \frac{\partial \mathscr{C}}{\partial \dot{\gamma}_{ij}}, \tag{5}$$

where γ_{ij} denotes a strain tensor, $\mathscr{W}$ denotes a general strain energy potential, and $\mathscr{C}$ denotes a quadratic Rayleigh damping function. The string is considered to be perfectly flexible, or equivalently, the only stress present in the string is the uni-axial stress t^{11}, the string being unable to support any other stress components. From equation (5), the perfectly flexible assumption requires that $\mathscr{W} = \mathscr{W}(\gamma_{11})$ and $\mathscr{C} = \mathscr{C}(\dot{\gamma}_{11})$ only. Thus, expressing $\mathscr{W}(\gamma_{11})$ by its Taylor expansion, the constitutive relationship can be stated as

$$t^{11} = \frac{T_0}{A^{\mathrm{T}}} + \left(k_1 + C\frac{\partial}{\partial t}\right)\gamma_{11} + k_2\gamma_{11}^2 + k_3\gamma_{11}^3 + O(\gamma_{11}^4), \tag{6}$$

where T_0 is the initial string tension, k_1 is the elastic modulus, and k_2 and k_3 are non-linear moduli. The Kelvin–Voigt dissipation constant is denoted by C. All material constants appearing in equation (6) are measured relative to the tensioned configuration.

To complete the string model, the functional form of the strain γ_{11} is defined. The exact line element (or Hookean) strain is used such that

$$\gamma_{11} = \frac{\sqrt{G_{11}}\,\mathrm{d}x^1 - \mathrm{d}x_1}{\mathrm{d}x_1} = \sqrt{(1 + u_{1,1})^2 + u_{2,1}^2 + u_{3,1}^2} - 1, \tag{7}$$

where the scalar product between the covariant base vectors,

$$\mathbf{G}_{ij} \equiv \mathbf{G}_i \cdot \mathbf{G}_j = \delta_{ij} + u_{i,j} + u_{j,i} + u_{m,i}u_{m,j}, \tag{8}$$

has been implemented in equation (7).

Substituting equations (3) and equations (6) and (7) into equation (1), noting A^{T} is independent from x_1 for a homogeneous string, and keeping terms to cubic order in the displacements, their spatial and their temporal derivatives, the u_1, u_2, and u_3 equations appear in the formulation as

$$\begin{aligned}
\rho^{\mathrm{T}}\ddot{u}_1 = {} & \frac{\alpha_1 P}{A^{\mathrm{T}}}\delta\left(x_1 - \frac{L}{2}\right) + \left(\frac{T_0}{A^{\mathrm{T}}} + k_1 + C\frac{\partial}{\partial t}\right)u_{1,11} - c_1\rho^{\mathrm{T}}\dot{u}_1 - \beta_1\rho^{\mathrm{T}}g \\
& + \left(k_1 + C\frac{\partial}{\partial t}\right)\left(u_{1,1}^2 + \frac{1}{2}u_{2,1}^2 + \frac{1}{2}u_{3,1}^2\right)_{,1} \\
& - \left(\left(u_{1,1} + \frac{1}{2}u_{2,1}^2 + \frac{1}{2}u_{3,1}^2\right)C\frac{\partial}{\partial t}u_{1,1}\right)_{,1} \\
& + k_2(u_{1,1}^2)_{,1} + (k_2 + k_3)(u_{1,1}^3)_{,1} + k_2(u_{1,1}(u_{2,1}^2 + u_{3,1}^2))_{,1},
\end{aligned} \tag{9}$$

$$\begin{aligned}
\rho^{\mathrm{T}}\ddot{u}_2 = {} & \frac{\alpha_2 P}{A^{\mathrm{T}}}\delta\left(x_1 - \frac{L}{2}\right) - \beta_2\rho^{\mathrm{T}}g + \frac{T_0}{A^{\mathrm{T}}}u_{2,11} - c_2\rho^{\mathrm{T}}\dot{u}_2 + k_2(u_{2,1}u_{1,1}^2)_{,1} \\
& + \left(u_{2,1}\left(k_1 + C\frac{\partial}{\partial t}\right)\left(u_{1,1} + \frac{1}{2}u_{2,1}^2 + \frac{1}{2}u_{3,1}^2\right)\right)_{,1},
\end{aligned} \tag{10}$$

$$\rho^{\mathrm{T}}\ddot{u}_3 = \frac{T_0}{A^{\mathrm{T}}}u_{3,11} - c_3\rho^{\mathrm{T}}\dot{u}_3 + k_2(u_{3,1}u_{1,1}^2)_{,1}$$

$$+ \left(u_{3,1}\left(k_1 + C\frac{\partial}{\partial t}\right)\left(u_{1,1} + \frac{1}{2}u_{2,1}^2 + \frac{1}{2}u_{3,1}^2\right)\right)_{,1}. \tag{11}$$

Lastly, a convenient non-dimensionalization is introduced followed by an ordering of the damping and excitation. Defining the longitudinal and transverse wave speeds (and similar quantities),

$$\frac{T_0}{\rho^{\mathrm{T}}A^{\mathrm{T}}} = s_2^2, \quad \frac{k_1}{\rho^{\mathrm{T}}} = s_1^2, \quad \frac{k_2}{\rho^{\mathrm{T}}} = a_2 s_1^2, \quad \frac{k_3}{\rho^{\mathrm{T}}} = a_3 s_1^2, \quad s_1^2 + s_2^2 = \hat{r}^2 s_2^2, \tag{12}$$

the following non-dimensionalization can be specified:

$$x_1 = Lx^*, \quad t = \frac{t^*}{\Omega}, \quad u_1 = \varepsilon L u^*, \quad u_2 = \varepsilon L v^*, \quad u_3 = \varepsilon L w^*,$$

$$C = \varepsilon\frac{\rho^{\mathrm{T}}L^2}{\Omega}C^*, \quad c_1 = \varepsilon\frac{1}{\Omega}c_1^*, \quad c_2 = \varepsilon\frac{1}{\Omega}c_2^*, \quad c_3 = \varepsilon\frac{1}{\Omega}c_3^*,$$

$$P = \varepsilon^2\rho^{\mathrm{T}}A^{\mathrm{T}}L^2P^*, \qquad g = \varepsilon^2 L g^*, \tag{13}$$

where it is noted that

$$H(L(x^* - \tfrac{1}{2})) = H(x^* - \tfrac{1}{2}), \qquad \delta(L(x^* - \tfrac{1}{2})) = \frac{1}{L}\delta(x^* - \tfrac{1}{2}).$$

The small parameter ε is not a physical quantity in the system, and is instead used as a book-marking device. The only requirement associated with the use of this parameter is that the amplitude of the displacements must be small.

Substituting equation (13) into equations (9)–(11) and retaining terms up $O(\varepsilon^2)$, the system equations are restated as

$$\Omega^2\frac{\partial^2 u}{\partial t^2} = \varepsilon\alpha_1 P\delta\left(x - \frac{1}{2}\right) + \left(\frac{\hat{r}^2 s_2^2}{L^2} + \varepsilon C\frac{\partial}{\partial t}\right)\frac{\partial^2 u}{\partial x^2} - \varepsilon c_1\frac{\partial u}{\partial t} - \varepsilon\beta_1 g$$

$$+ \varepsilon\left(\frac{(\hat{r}^2 - 1)s_2^2}{L^2} + \varepsilon C\frac{\partial}{\partial t}\right)\frac{\partial}{\partial x}\left(\left(\frac{\partial u}{\partial x}\right)^2 + \frac{1}{2}\left(\frac{\partial v}{\partial x}\right)^2 + \frac{1}{2}\left(\frac{\partial w}{\partial x}\right)^2\right)$$

$$+ \varepsilon a_2\frac{(\hat{r}^2 - 1)s_2^2}{L^2}\frac{\partial}{\partial x}\left(\left(\frac{\partial u}{\partial x}\right)^2\right)$$

$$+ \varepsilon^2 a_2\frac{(\hat{r}^2 - 1)s_2^2}{L^2}\frac{\partial}{\partial x}\left(\frac{\partial u}{\partial x}\left(\left(\frac{\partial v}{\partial x}\right)^2 + \left(\frac{\partial w}{\partial x}\right)^2\right)\right)$$

$$- \varepsilon^2 C\frac{\partial}{\partial x}\left(\frac{\partial u}{\partial x}\frac{\partial^2 u}{\partial x\,\partial t}\right) + \varepsilon^2(a_2 + a_3)\frac{(\hat{r}^2 - 1)s_2^2}{L^2}\frac{\partial}{\partial x}\left(\left(\frac{\partial u}{\partial x}\right)^3\right), \tag{14}$$

$$\Omega^2 \frac{\partial^2 v}{\partial t^2} = \varepsilon \alpha_2 P \delta\left(x - \frac{1}{2}\right) + \frac{s_2^2}{L^2}\frac{\partial^2 v}{\partial x^2} - \varepsilon \beta_2 g - \varepsilon c_2 \frac{\partial v}{\partial t}$$
$$+ \varepsilon \frac{\partial}{\partial x}\left(\frac{\partial v}{\partial x}\left(\frac{(\hat{r}^2 - 1)s_2^2}{L^2} + \varepsilon C \frac{\partial}{\partial t}\right)\left(\frac{\partial u}{\partial x} + \varepsilon \frac{1}{2}\left(\frac{\partial v}{\partial x}\right)^2 + \varepsilon \frac{1}{2}\left(\frac{\partial w}{\partial x}\right)^2\right)\right)$$
$$+ \varepsilon^2 a_2 \frac{(\hat{r}^2 - 1)s_2^2}{L^2}\frac{\partial}{\partial x}\left(\frac{\partial v}{\partial x}\left(\frac{\partial u}{\partial x}\right)^2\right), \tag{15}$$

$$\Omega^2 \frac{\partial^2 w}{\partial t^2} = \frac{s_2^2}{L^2}\frac{\partial^2 w}{\partial x^2} - \varepsilon c_3 \frac{\partial w}{\partial t}$$
$$+ \varepsilon \frac{\partial}{\partial x}\left(\frac{\partial w}{\partial x}\left(\frac{(\hat{r}^2 - 1)s_2^2}{L^2} + \varepsilon C \frac{\partial}{\partial t}\right)\left(\frac{\partial u}{\partial x} + \varepsilon \frac{1}{2}\left(\frac{\partial v}{\partial x}\right)^2 + \varepsilon \frac{1}{2}\left(\frac{\partial w}{\partial x}\right)^2\right)\right)$$
$$+ \varepsilon^2 a_2 \frac{(\hat{r}^2 - 1)s_2^2}{L^2}\frac{\partial}{\partial x}\left(\frac{\partial w}{\partial x}\left(\frac{\partial u}{\partial x}\right)^2\right), \tag{16}$$

where the $*$ notation has been dropped.

3. EVOLUTION EQUATIONS

When an internal resonance mechanism exists between transverse and longitudinal modes of the string, transverse excitation can lead to significant longitudinal motions, whereby the effects of material non-linearities increase in importance. In what follows, full coupling mechanisms are identified which lead to interactions between certain longitudinal and transverse modes. After identifying the possible mechanisms, the resonant mechanism corresponding to coupled cubic terms is studied in further detail.

The midpoint forcing of the string is now defined as

$$P = p \cos(\Omega t), \tag{17}$$

where the excitation frequency Ω is considered to be detuned from a system longitudinal or transverse natural frequency,

$$\Omega^2 = j^2 \hat{r}^2 \frac{s_2^2}{L^2} + \varepsilon\sigma = j^2 \hat{r}^2 \omega_i^2 + \varepsilon(\sigma_1 + \varepsilon\sigma_2), \tag{18}$$

and the ratio parameter $\hat{r}$ is considered to be detuned from an integer value,

$$\hat{r}^2 = r^2 + \varepsilon\sigma_r. \tag{19}$$

For example, if $j = N\pi$ where N is an integer, then Ω is near the Nth linear natural frequency of a longitudinal mode. If $j = I\pi/r$, where I is an integer, then Ω is near the Ith transverse linear natural frequency and, furthermore, if $I/r = K$ is itself an integer, Ω is also near the Kth linear natural frequency of a longitudinal mode. In this way, P is likely to *directly* excite a single longitudinal mode, a single transverse mode, or both a longitudinal and a transverse mode. It is also possible for P to *indirectly* excite integer multiples of these modes

due to the non-linearities present in equations (14)–(16), so-called super-harmonically excited modes.

Similar to the frequency, viscoelastic and linear damping are ordered to appear at all ε-orders,

$$C = C_1 + \varepsilon C_2, \quad c_1 = c_{11} + \varepsilon c_{12}, \quad c_2 = c_{21} + \varepsilon c_{22}, \quad c_3 = c_{31} + \varepsilon c_{32}. \tag{20}$$

An analysis using the multiple scales method directly applied to the governing partial differential equations (14)–(16) is begun next. The analysis is completed to $O(\varepsilon^2)$. First, separate time scales are introduced at each $O(\varepsilon)$, along with an ordered expansion for the displacements u, v, and w as follows:

$$t = T_0 + \varepsilon T_0 + \varepsilon^2 T_0 + O(\varepsilon^3) = T_0 + T_1 + T_2 + O(\varepsilon^3), \tag{21}$$

$$u(x,t) = u_0(x, T_0, T_1, T_2) + \varepsilon u_1(x, T_0, T_1, T_2) + \varepsilon^2 u_2(x, T_0, T_1, T_2) + O(\varepsilon^3), \tag{22}$$

$$v(x,t) = v_0(x, T_0, T_1, T_2) + \varepsilon v_1(x, T_0, T_1, T_2) + \varepsilon^2 v_2(x, T_0, T_1, T_2) + O(\varepsilon^3), \tag{23}$$

$$w(x,t) = w_0(x, T_0, T_1, T_2) + \varepsilon w_1(x, T_0, T_1, T_2) + \varepsilon^2 w_2(x, T_0, T_1, T_2) + O(\varepsilon^3), \tag{24}$$

$$D_0 = \frac{\partial}{\partial T_0}, \qquad D_1 = \frac{\partial}{\partial T_1}, \qquad D_2 = \frac{\partial}{\partial T_2}, \tag{25}$$

where

$$\frac{\partial}{\partial t} = D_0 + \varepsilon D_1 + \varepsilon^2 D_2 + O(\varepsilon^3). \tag{26}$$

Substitution of equations (17)–(26) into equations (14)–(16) and equating coefficients of like $O(\varepsilon)$, yields the ordered equations

$$D_0^2 u_0 - \frac{1}{j^2}\frac{\partial^2 u_0}{\partial x^2} = 0, \qquad D_0^2 v_0 - \frac{1}{r^2 j^2}\frac{\partial^2 v_0}{\partial x^2} = 0, \tag{27,28}$$

$$D_0^2 w_0 - \frac{1}{r^2 j^2}\frac{\partial^2 w_0}{\partial x^2} = 0, \tag{29}$$

at $O(\varepsilon^0)$ and

$$\begin{aligned} j^2 r^2 \omega_t^2 D_0^2 u_1 - r^2 \omega_t^2 \frac{\partial^2 u_1}{\partial x^2} = {} & \frac{\alpha_1 p}{2}[e^{iT_0} + cc]\delta\left(x - \frac{1}{2}\right) - \beta_1 g \\ & - [(\sigma_1 + j^2 \sigma_r \omega_t^2) D_0^2 + c_{11} D_0 + 2 j^2 r^2 \omega_t^2 D_0 D_1] u_0 \\ & + \left[(2a_2 + 2)(r^2 - 1)\omega_t^2 \frac{\partial u_0}{\partial x}\frac{\partial^2 u_0}{\partial x^2}\right] + (C_1 D_0 + \sigma_r \omega_t^2)\frac{\partial^2 u_0}{\partial x^2} \\ & + (r^2 - 1)\omega_t^2 \left[\frac{\partial v_0}{\partial x}\frac{\partial^2 v_0}{\partial x^2} + \frac{\partial w_0}{\partial x}\frac{\partial^2 w_0}{\partial x^2}\right], \end{aligned} \tag{30}$$

$$j^2r^2\omega_t^2D_0^2v_1 - \omega_t^2\frac{\partial^2 v_1}{\partial x^2} = \frac{\alpha_2 p}{2}[e^{iT_0} + cc]\delta\left(x - \frac{1}{2}\right) - \beta_2 g$$
$$- [(\sigma_1 + j^2\sigma_r\omega_t^2)D_0^2 + c_{21}D_0 + 2j^2r^2\omega_t^2D_0D_1]v_0$$
$$+ (r^2 - 1)\omega_t^2\left[\frac{\partial u_0}{\partial x}\frac{\partial^2 v_0}{\partial x^2} + \frac{\partial v_0}{\partial x}\frac{\partial^2 u_0}{\partial x^2}\right], \tag{31}$$

$$j^2r^2\omega_t^2D_0^2w_1 - \omega_t^2\frac{\partial^2 w_1}{\partial x^2} = [(\sigma_1 + j^2\sigma_r\omega_t^2)D_0^2 + c_{31}D_0 + 2j^2r^2\omega_t^2D_0D_1]w_0$$
$$+ (r^2 - 1)\omega_t^2\left[\frac{\partial u_0}{\partial x}\frac{\partial^2 w_0}{\partial x^2} + \frac{\partial w_0}{\partial x}\frac{\partial^2 u_0}{\partial x^2}\right], \tag{32}$$

at $O(\varepsilon^1)$. The $O(\varepsilon^2)$ equations are given in Appendix A. The corresponding boundary conditions for each order are determined from equation (4) and equations (21)–(24),

$$u_0(0, T_0, T_1, T_2) = u_0(1, T_0, T_1, T_2) = \cdots = u_2(1, \cdots) = 0,$$
$$v_0(0, T_0, T_1, T_2) = v_0(1, T_0, T_1, T_2) = \cdots = v_2(1, \cdots) = 0,$$
$$w_0(0, T_0, T_1, T_2) = w_0(1, T_0, T_1, T_2) = \cdots = w_2(1, \cdots) = 0. \tag{33}$$

The general solutions to the linear ε^0 equations (27)–(29) satisfying the homogeneous boundary conditions contained in equation (33) are given by

$$u_0 = \sum_{m=1}^{\infty}(A_{1m}e^{i(m\pi/j)T_0} + cc)\sin m\pi x, \tag{34}$$

$$v_0 = \sum_{m=1}^{\infty}(A_{2m}e^{i(m\pi/rj)T_0} + cc)\sin m\pi x, \tag{35}$$

$$w_0 = \sum_{m=1}^{\infty}(A_{3m}e^{i(m\pi/rj)T_0} + cc)\sin m\pi x, \tag{36}$$

where cc denotes the complex conjugate of the preceding terms and information about the modal amplitudes $A_{im} = A_{im}(T_1, T_2)$ is to be determined at the next ε-order. These solutions are now used to update the $O(\varepsilon^1)$ equations.

Since the homogeneous parts of equations (30)–(32) each have a non-trivial solution satisfying the homogeneous boundary conditions (33), solvability conditions must be imposed on the inhomogeneities in order to insure the existence of solutions. Specifically, secular terms must be eliminated. Since the string's stiffness operators are self-adjoint and the boundary conditions are homogeneous, secular terms are identified as those terms which have *both* temporal frequency equal to an eigenfrequency and a non-zero projection on to the corresponding spatial eigenfunction.

For the u_1 equation (30), elimination of secular terms begins by isolating all terms in the inhomogeneity with temporal dependence $e^{i(l\pi/j)T_0}$:

$$\frac{\alpha_1 p}{2}\delta\left(\frac{l\pi}{j} - 1\right)\delta\left(x - \frac{1}{2}\right) - \left[-\sigma_1\left(\frac{l\pi}{j}\right)^2 + i\left(\frac{l\pi}{j}c_{11} + (l\pi)^2\frac{l\pi}{j}C_1\right) - i2jl\pi r^2\omega_t^2D_1\right]A_{1l}\sin l\pi x$$
$$- (2a_2 + 2)(r^2 - 1)\omega_t^2\sum_{n=1}^{\infty}[(l - n)n^2\pi^3A_{1(l-n)}A_{1n}\cos(l - n)\pi x\sin n\pi x$$

$$+ (l+n)n^2\pi^3 A_{1(l+n)}\bar{A}_{1n}\cos(l+n)\pi x \sin n\pi x$$

$$+ (n-l)n^2\pi^3 \bar{A}_{1(n-l)}A_{1n}\cos(n-l)\pi x \sin n\pi x]$$

$$- (r^2-1)\omega_t^2 \sum_{K=2,3}\sum_{n=1}^{\infty}[(rl-n)n^2\pi^3 A_{K(rl-n)}A_{Kn}\cos(rl-n)\pi x \sin n\pi x$$

$$+ (rl+n)n^2\pi^3 A_{K(rl+n)}\bar{A}_{Kn}\cos(rl+n)\pi x \sin n\pi x$$

$$+ (n-rl)n^2\pi^3 \bar{A}_{K(n-rl)}A_{Kn}\cos(n-rl)\pi x \sin n\pi x]. \tag{37}$$

The final step in identifying the secular terms is to set the inner product of equation (37) with $\sin l\pi x$ to zero, yielding the solvability condition:

$$\alpha_1 p\delta\left(\frac{l\pi}{j}-1\right)\sin\frac{l\pi}{2} - \left[-\sigma_1\left(\frac{l\pi}{j}\right)^2 + i\frac{l\pi}{j}(c_{11}+(l\pi)^2 C_1 + 2j^2r^2\omega_t^2 D_1)\right]A_{1l}$$

$$-(a_2+1)(r^2-1)\omega_t^2\sum_{n=1}^{\infty}(nl^2+n^2l)\pi^3 A_{1(l+n)}\bar{A}_{1n} + \sum_{n=1}^{l-1}(l-n)n^2\pi^3 A_{1(l-n)}A_{1n}$$

$$-\frac{(r^2-1)^2\omega_t^2}{8}\pi^3[A_{2(\frac{r-1}{2}l)}A_{2(\frac{r+1}{2}l)} + A_{3(\frac{r-1}{2}l)}A_{3(\frac{r+1}{2}l)}] = 0. \tag{38}$$

A similar procedure is followed to determine the secular terms in equations (31)–(32), with the resulting solvability conditions given by

$$\alpha_2 p\delta(l\pi - jr)\sin\frac{l\pi}{2} - \left[-(\sigma_1 + j^2\sigma_r\omega_t^2)\left(\frac{l\pi}{jr}\right)^2 + i\frac{l\pi}{jr}(c_{21}+2jr^2\omega_t^2 D_1)\right]A_{2l}$$

$$-\frac{(r^2-1)\omega_t^2}{2}\pi^3\left[\frac{2(r-1)}{(r+1)^2}l^3 A_{1(\frac{2l}{r+1})}\bar{A}_{2(\frac{r-1}{r+1}l)} + \frac{2(r+1)}{(r-1)^2}l^3 A_{1(\frac{2l}{r-1})}\bar{A}_{2(\frac{r+1}{r-1}l)}\right]$$

$$= 0, \tag{39}$$

$$-\left[-(\sigma_1 + j^2\sigma_r\omega_t^2)\left(\frac{l\pi}{jr}\right)^2 + i\frac{l\pi}{jr}(c_{31}+2jr^2\omega_t^2 D_1)\right]A_{3l}$$

$$-\frac{(r^2-1)\omega_t^2}{2}\pi^3\left[\frac{2(r-1)}{(r+1)^2}l^3 A_{1(\frac{2l}{r+1})}\bar{A}_{3(\frac{r-1}{r+1}l)} + \frac{2(r+1)}{(r-1)^2}l^3 A_{1(\frac{2l}{r-1})}\bar{A}_{3(\frac{r+1}{r-1}l)}\right]$$

$$= 0, \tag{40}$$

4. INTERNAL RESONANCE MECHANISMS

4.1. QUADRATIC

An inspection of equations (38)–(40) reveals many possible internal resonance mechanisms exhibited by quadratic coupling terms. These will be referred to as quadratically induced resonance mechanisms. First, when the ratio of the longitudinal

natural frequency to the transverse natural frequency is odd (i.e., r odd), resonant interactions can occur between the Lth longitudinal mode and *two* transverse modes, the $(((r+1)/2)L)$th and the $(((r-1)/2)L)$th. When r is even, the same interactions can occur, except with even numbered Lth longitudinal modes only. These interactions occur in each secular equation (see the final terms in each of equations (38)–(40)), and are thus fully coupled. It is also observed that in-plane and out-of-plane transverse modes are not directly coupled at quadratic order, and quadratically initiated whirling motions, to this order, can only occur if longitudinal modes are excited. Finally, it is noted (but not shown here) that these same modal combinations involved in quadratically induced resonance mechanisms are also involved in cubically induced resonance mechanisms at the next ε order, including directly coupled whirling motions, which should serve to reinforce their effect. An analysis to $O(\varepsilon^2)$ has been completed, but not fixed points of the autonomous evolution equations were found corresponding to the internal resonance mechanism. In the physical system, this indicates that periodic solutions will not arise in which excitation of either the $(((r+1)/2)L)$th or the $(((r-1)/2)L)$th transverse mode leads to response in the Lth longitudinal mode, or *vice versa.* The quadratic mechanisms will not be discussed further, and instead, the remainder of this study will focus on cubically induced internal resonance mechanisms.

4.2. CUBIC

The spatial and temporal frequency content of the cubic coupling expressions is examined next and the secular terms arising at $O(\varepsilon^2)$ are determined. Cubically induced internal resonance mechanisms between a *single* longitudinal mode and a *single* transverse mode are likely due to the expressions $\partial/\partial x(\partial u_0/\partial x(\partial v_0/\partial x)^2)$ (in the longitudinal $O(\varepsilon^2)$ equation) and $\partial/\partial x(\partial v_0/\partial x(\partial u_0/\partial x)^2)$, $\partial/\partial x(\partial w_0/\partial x(\partial u_0/\partial x)^2)$ (in the transverse $O(\varepsilon^2)$ equations). Specifically, these expressions lead to secular terms between the mth transverse mode and the nth longitudinal mode whenever $m = nr$. For example, the $O(\varepsilon^2)$ longitudinal expression leads to the secular term

$$-\frac{(n\pi)^4 r^2}{2}\bar{A}_{1n}A_{2nr}^2 e^{i(n\pi/j)T_0}\sin n\pi x, \tag{41}$$

while the in-plane and out-of-plane transverse expressions lead to the secular terms

$$-\frac{(n\pi)^4 r^2}{2}\bar{A}_{2rn}A_{1n}^2 e^{i(n\pi/j)T_0}\sin nr\pi x, \tag{42}$$

$$-\frac{(n\pi)^4 r^2}{2}\bar{A}_{3rn}A_{1n}^2 e^{i(n\pi/j)T_0}\sin nr\pi x \tag{43}$$

respectively. Similar to the quadratic mechanisms identified, the cubic mechanisms are fully coupled.

To study the cubic interactions at a finite state size, a modal truncation is introduced. Longitudinal and transverse modes which are either not directly excited nor involved in an internal resonance are likely to be of negligible importance. Here, we choose to consider direct forcing of the (rN)th in-plane transverse mode such that $\alpha_2 \neq 0$ and $j = N\pi$. With this choice, only the Nth longitudinal and the (rN)th transverse modes are retained in equations (34)–(36) and equations (38)–(40) for the remainder of the analysis.

Following introduction of the modal truncation into the multiple scales analysis, the particular solutions to equations (30)–(32) are found before addressing the $O(\varepsilon^2)$ equations. The u_1 particular solution satisfies both the inhomogeneities remaining after subtraction of equation (37) from equation (30) (similarly for v_1, w_1 particular solutions) *and* the inhomogeneities resulting from terms in equation (37) orthogonal to the spatial eigenfunction $\sin N\pi x$ ($\sin Nr\pi x$ for analogous v_1, w_1 equations). With these considerations, the particular solutions for the u_1, v_1, and w_1 equations are denoted as the complex conjugate pairs ($U_1(x, T_0, T_1, T_2)$, $\bar{U}_1(x, T_0, T_1, T_2)$), ($V_1(x, T_0, T_1, T_2)$, $\bar{V}_1(x, T_0, T_1, T_2)$), and ($W_1(x, T_0, T_1, T_2)$, $\bar{W}_1(x, T_0, T_1, T_2)$), respectively, and are given by

$$\begin{aligned} U_1 = {} & \frac{\beta_1 g}{4r^2\omega_t^2}(x^2 - x) + \underbrace{\sum_{m=1}^{\infty}}_{m \neq N} \frac{\alpha_1 p \sin m\pi/2}{r^2\pi^2\omega_t^2(m^2 - N^2)} e^{iT_0} \sin m\pi x \\ & - \frac{(a_2 + 1)(r^2 - 1)N\pi}{4r^2} A_{1N}\bar{A}_{1N} \sin 2N\pi x \\ & - \frac{rN\pi}{8}[A_{2rN}^2 + A_{3rN}^2] e^{i2T_0} \sin 2rN\pi x \\ & - \frac{(r^2 - 1)N\pi}{8r}[A_{2rN}\bar{A}_{2rN} + A_{3rN}\bar{A}_{3rN}] \sin 2rN\pi x, \end{aligned} \tag{44}$$

$$\begin{aligned} V_1 = {} & \frac{\beta_2 g}{4\omega_t^2}(x^2 - x) + \underbrace{\sum_{m=1}^{\infty}}_{m \neq rN} \frac{\alpha_2 p \sin m\pi/2}{\pi^2\omega_t^2(m^2 - (rN)^2)} e^{iT_0} \sin m\pi x \\ & + \left(\frac{\pi(r + 1)^2 rN}{2(3r + 1)} \sin((r + 1)N\pi x) \right. \\ & \left. + \frac{\pi(r - 1)^2 rN}{2(3r - 1)} \sin((r - 1)N\pi x) \right) A_{1N}A_{2rN} e^{i2T_0} \\ & - \left(\frac{1}{2}\pi rN(r - 1) \sin((r + 1)N\pi x) \right. \\ & \left. + \frac{1}{2}\pi rN(r + 1) \sin((r - 1)N\pi x) \right) A_{1N}\bar{A}_{2rN}, \end{aligned} \tag{45}$$

$$\begin{aligned} W_1 = {} & \left(\frac{\pi(r + 1)^2 rN}{2(3r + 1)} \sin((r + 1)N\pi x) \right. \\ & \left. + \frac{\pi(r - 1)^2 rN}{2(3r - 1)} \sin((r - 1)N\pi x) \right) A_{1N}A_{3rN} e^{i2T_0} \\ & - \left(\frac{1}{2}\pi rN(r - 1) \sin((r + 1)N\pi x) \right. \\ & \left. + \frac{1}{2}\pi rN(r + 1) \sin((r - 1)N\pi x) \right) A_{1N}\bar{A}_{3rN}. \end{aligned} \tag{46}$$

Note that *non-resonant* longitudinal motions can be captured by setting A_{1N} to zero and retaining only the particular solution for the longitudinal equation (44). This limiting case reveals that longitudinal motions are proportional to A_{2rN}^2 and A_{3rN}^2, and thus occur at twice the spatial and temporal frequency of the excited transverse mode, as proposed by Narasimha [1].

The procedure for eliminating secular terms in the $O(\varepsilon^2)$ equations follows closely that of the $O(\varepsilon^1)$ equations. Specifically, the approach adopted is that of Lee and Perkins [9] in which the particular solutions are substituted into the $O(\varepsilon^2)$ equations, $O(\varepsilon^1)$ derivatives (D_1) are set to zero, and expressions for the $O(\varepsilon^2)$ derivative (D_2) of the modal amplitudes are obtained. This is one of several approaches currently existing in the literature; see reference [14] for a discussion. Appendix B lists the $O(\varepsilon^2)$ solvability conditions and describes the reconstitution procedure invoked to determine the evolution equations.

The reconstitution procedure of Appendix B yields the autonomous evolution equations

$$\begin{aligned}\frac{1}{L}\frac{\mathrm{d}A_{1N}}{\mathrm{d}t} = \frac{-\mathrm{i}\Omega}{2(\pi\omega_t N r)^2}\Bigg[&\frac{\alpha_1 p}{\rho^{\mathrm{T}}A^{\mathrm{T}}L^2}\sin\frac{N\pi}{2} + \left(\hat{\sigma} - \mathrm{i}\left(\Omega c_1 + \frac{\Omega N^2\pi^2}{\rho^{T2}L^2}C\right)\right)\frac{A_{1N}}{L}\\ &+ \frac{(r^2-1)\pi^4N^4\omega_t^2}{4r^2}(4(r^2-1)(a_2+1)^2 - 9(a_2+a_3)r^2)\frac{A_{1N}|A_{1N}|^2}{L^3}\\ &+ \frac{r^2(r^2-1)\pi^4N^4\omega_t^2}{2}(r^2-a_2-1)\frac{\bar{A}_{1N}(A_{2rN}^2+A_{3rN}^2)}{L^3}\\ &+ \frac{r^2(r^2-1)\pi^4N^4\omega_t^2}{9r^2-1}(3r^4-(9a_2+8)r^2+a_2+1)\frac{A_{1N}(|A_{2rN}|^2+|A_{3rN}|^2)}{L^3}\Bigg], \quad (47)\end{aligned}$$

$$\begin{aligned}\frac{1}{L}\frac{\mathrm{d}A_{2rN}}{\mathrm{d}t} = \frac{-\mathrm{i}\Omega}{2(\pi\omega_t N r)^2}\Bigg[&\frac{\alpha_2 p}{\rho^{\mathrm{T}}A^{\mathrm{T}}L^2}\sin\frac{N\pi r}{2} + (\hat{\sigma} + N^2\pi^2\omega_t^2\hat{\sigma}_r - \mathrm{i}\Omega c_2)\frac{A_{2rN}}{L}\\ &- \frac{(r^2-1)\pi^4N^4r^2\omega_t^2}{8}\Bigg((7r^2+2)\frac{A_{2rN}|A_{2rN}|^2}{L^3} + (4r^2+2)\frac{A_{2rN}|A_{3rN}|^2}{L^3}\\ &+ 3r^2\frac{\bar{A}_{2rN}A_{3rN}^2}{L^3} - 4(r^2-a_2-1)\frac{\bar{A}_{2rN}A_{1N}^2}{L^3}\Bigg)\\ &+ \frac{(r^2-1)\pi^4N^4r^2\omega_t^2}{9r^2-1}(3r^4-(9a_2+8)r^2+a_2+1)\frac{A_{2rN}|A_{1N}|^2}{L^3}\Bigg], \quad (48)\end{aligned}$$

$$\begin{aligned}\frac{1}{L}\frac{\mathrm{d}A_{3rN}}{\mathrm{d}t} = \frac{-\mathrm{i}\Omega}{2(\pi\omega_t N r)^2}\Bigg[&(\hat{\sigma} + N^2\pi^2\omega_t^2\hat{\sigma}_r - \mathrm{i}\Omega c_3)\frac{A_{3rN}}{L}\\ &- \frac{(r^2-1)\pi^4N^4r^2\omega_t^2}{8}\Bigg((7r^2+2)\frac{A_{3rN}|A_{3rN}|^2}{L^3} + (4r^2+2)\frac{A_{3rN}|A_{2rN}|^2}{L^3}\\ &+ 3r^2\frac{\bar{A}_{3rN}A_{2rN}^2}{L^3} - 4(r^2-a_2-1)\frac{\bar{A}_{3rN}A_{1N}^2}{L^3}\Bigg)\\ &+ \frac{(r^2-1)\pi^4N^4r^2\omega_t^2}{9r^2-1}(3r^4-(9a_2+8)r^2+a_2+1)\frac{A_{3rN}|A_{1N}|^2}{L^3}\Bigg], \quad (49)\end{aligned}$$

where $\hat{\sigma} = \varepsilon\sigma$ and $\hat{\sigma}_r = \varepsilon\sigma_r$ are small quantities.

5. RESULTS

The evolution equations of section 4.2 are analyzed in this section to determine equilibrium, periodic, and aperiodic solutions (and the stability of each) for example strings with a frequency ratio of $\hat{r} \approx 3$. For these strings, excitation of the third transverse mode may lead to resonant longitudinal motions at the first mode. This mechanism is studied by setting $r = 3$ and $N = 1$ in equations (47)–(49) and decomposing the complex modal amplitudes into their real and imaginary Cartesian components. The discussion of the results is limited primarily to internally resonant solutions ($A_{1N} \neq 0$), although the simple planar ($A_{1N} = A_{3rN} = 0$) and simple whirling ($A_{1N} = 0$; A_{2rN}, $A_{3rN} \neq 0$) solutions will be presented in some figures. These solutions are not discussed in detail here because they have been treated exhaustively in the studies cited in the introduction, and the present analysis reproduces their solutions with the same topological character. Fixed point solutions to the evolution equations are found by locating solution branches at various values of detuning $\hat{\sigma}$ (through initial guesses and subsequent iteration with a Newton–Raphson solver), and then following the branch with the aid of a continuation method [15], which also determines stability automatically using a local eigenvalue analysis. Periodic and aperiodic solutions to the evolution equations are found through numerical simulation [16].

5.1. FIXED POINT SOLUTIONS FOR EVOLUTION EQUATIONS

Depending on the strength of the material non-linearities, the stability and existence of the internally resonant solutions may be greatly influenced. Figure 2 presents frequency response curves (energy versus detuning) for two strings with different degrees of material non-linearity. Only fixed point solutions to the evolution equations (periodic solutions in the physical system) and their stability are shown in the figure. In the top two sub-figures, the string is characterized with non-zero linear material properties only, while the bottom two sub-figures correspond to a string characterized by $a_2 = 4$ and $a_3 = 6$. These two examples are discussed at fixed levels of damping and modal detuning $\hat{\sigma}_r$ (given in the caption of Figure 2) to illustrate the dominant character of possible solutions, but it should be noted that other choices for a_2, a_3 lead to further variation on the solutions, although to a lesser degree.

For the string characterized with a linear material description, several different fixed point solution branches exist, which correspond to a variety of string motions. Branches labelled $B1$–$B4$ in Figure 2 are summarized in Table B1 and are characterized according to their modal content. Branches involved in the internal resonance are those with a description preceded by *composite* and include planar and whirling solutions. These composite branches behave in a softening fashion, as witnessed by their bending towards decreasing $\hat{\sigma}$. For the linear material, each composite branch is unstable, and in fact, their existence causes the planar branch $B1$ to also be unstable in the region $-0{\cdot}897 < \hat{\sigma} < 0{\cdot}446$. This is in contrast to a string without resonantly excited longitudinal motions, where the planar solution would be stable in this same region. Hopf bifurcations, labelled $H1$–$H6$ in the figure, of which $H3$–$H6$ appear on the composite branches, are also found which locate detuning values at which limit cycles in the evolution equations appear. Local to $H1, H2, H3$, and $H6$, stable limit cycles exist, while local to $H4$ and $H6$, unstable limit cycles exist. More discussion on these and other non-equilibrium solutions follow below.

The fixed-point behavior of the example non-linear material string is topologically different from that of the linear material string. The same composite branches described above still exist, but now act in a (weakly) hardening manner, with their bifurcation

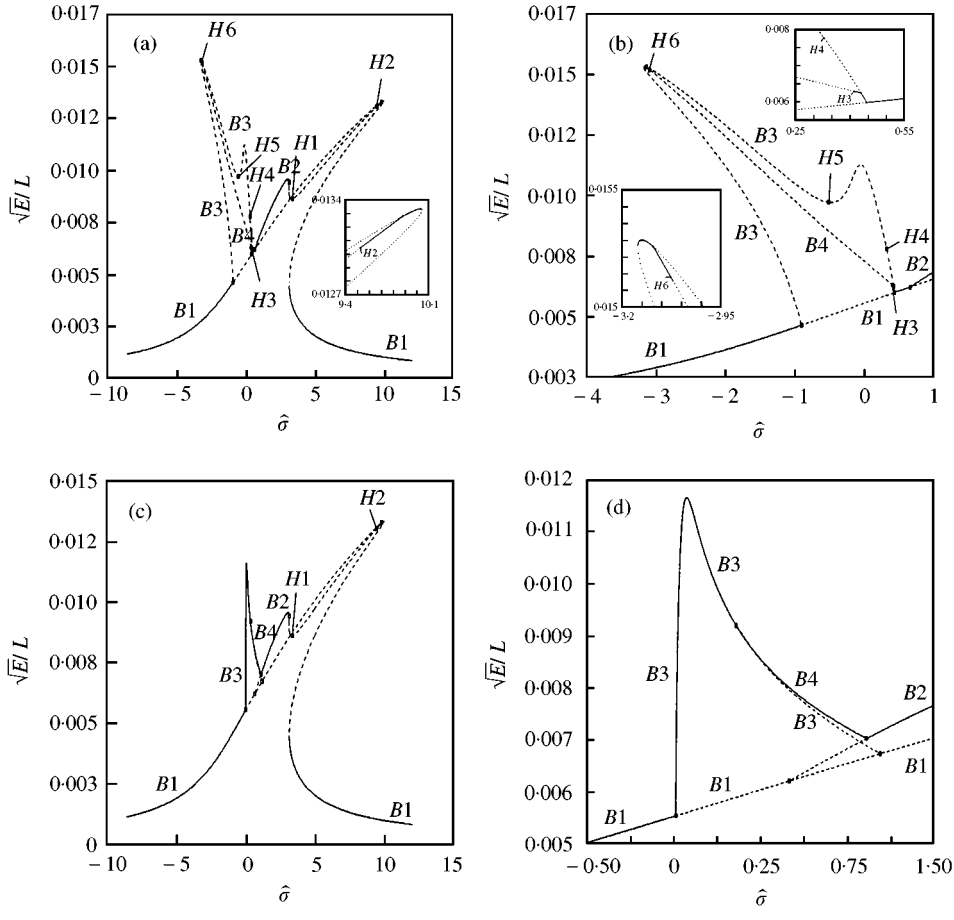

Figure 2. Fixed point solutions of the evolution equations used to generate modal energy versus detuning bifurcation diagrams for: (a)–(b) $a_2 = a_3 = 0$, and (c)–(d) $a_2 = 4$, $a_3 = 6$. Here $r = 3$, $N = 1$, $\hat{\sigma}_r = 0{\cdot}01$, $\omega_t = 1{\cdot}0$, $p/(\rho^{\mathrm{T}} A^{\mathrm{T}} L^2) = 0{\cdot}01$, and damping C, c_1, c_2, and c_3 are chosen to correspond to 0·11 per cent critical damping in the longitudinal direction and 0·27 per cent critical damping in the transverse directions. Local stability is indicated by line type: —, indicating stable solutions; - - - -, indicating unstable solutions.

locations away from the branch of simple planar solutions shifted in the direction of positive $\hat{\sigma}$. This shift causes a portion of the composite branches to coexist with part of the simple whirling branch, and destabilizes the overlapping portion of this branch. As in the linear material case, the segment of the simple planar branch coincident with the composite branches is unstable as well. Unlike the linear material, the $B3$ and $B4$ composite branches exhibit $\hat{\sigma}$-regions of stability, with the $B3$ branch losing stability at the $B3$–$B4$ bifurcation point. A further difference between the two examples is that no Hopf bifurcations exist on the composite branches of the non-linear material.

5.2. PERIODIC AND APERIODIC SOLUTIONS FOR EVOLUTION EQUATIONS

For the linear material string, the region $-0{\cdot}897 < \hat{\sigma} < 0{\cdot}446$ is devoid of stable fixed points, suggesting an increased likelihood of finding stable periodic and aperiodic solutions here. Numerical simulation of the evolution equations in the neighborhood of this region

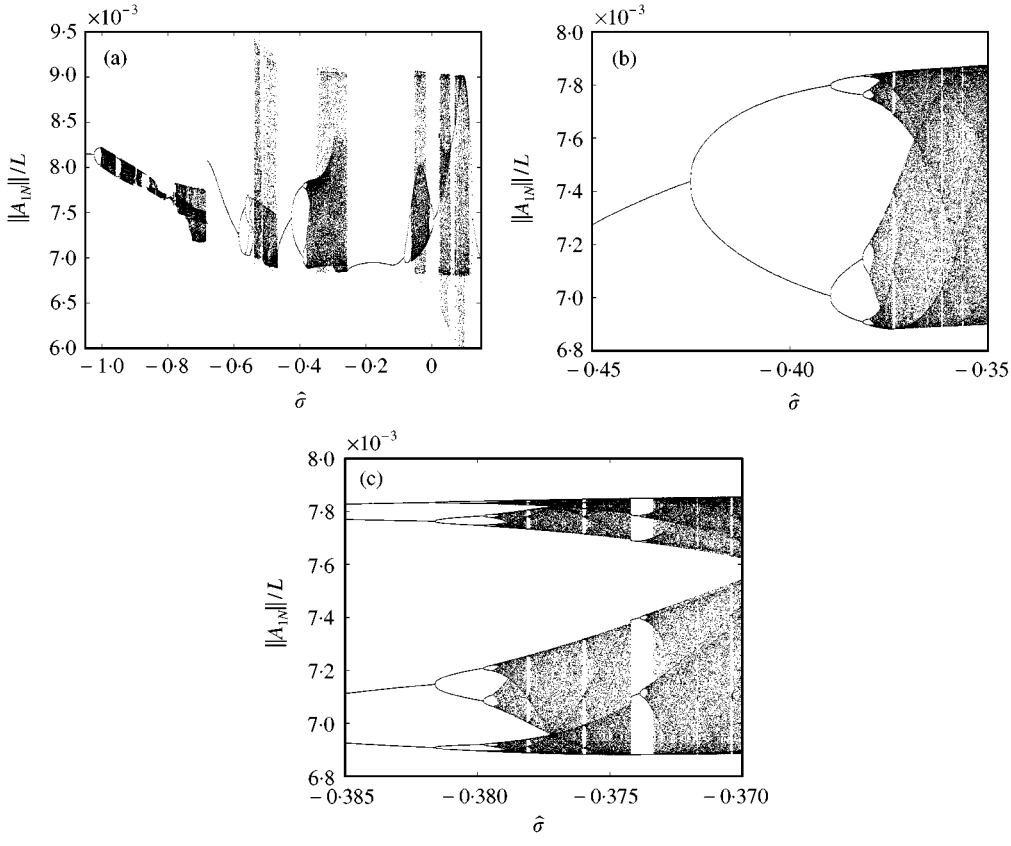

Figure 3. Bifurcation diagrams of $\|A_{1N}\|/L$ (at the Poincaré section $\mathrm{Re}\{A_{2rN}\} = 0$) versus detuning for the $a_2 = a_3 = 0$ system defined in the caption of Figure 2. Sub-figures (b)–(c) provide an increasingly detailed view of the bifurcation structure in the sub-region $-0{\cdot}45 < \hat{\sigma} < -0{\cdot}35$ of sub-figure (a).

does in fact reveal the existence of complex dynamics. At approximately $\hat{\sigma} = 1{\cdot}11$, a periodic composite whirling solution to the evolution equations (quasiperiodic in physical space) is first detected. Figure 3 presents bifurcation diagrams which record the evolution of this periodic solution as detuning $\hat{\sigma}$ is increased. The diagrams are generated by sampling the numerically calculated flow as it passes through the Poincaré section $\mathrm{Re}\{A_{2rN}\} = 0$, and recording the magnitude of A_{1N}. The initial periodic solution appears as a single point at $\hat{\sigma} = 1{\cdot}11$ in sub-figure (a). As $\hat{\sigma}$ is increased, this periodic solution persists until approximately $\hat{\sigma} = 1{\cdot}024$, at which point the period of the solution doubles and two points are recorded on the Poincaré section. A series of period bifurcations follows as $\hat{\sigma}$ is further increased, as shown in the sub-figure, leading to regions of complex dynamics interrupted by windows of periodic dynamics. For example, sub-figures (b)–(c) provide an increasingly detailed view of the region $-0{\cdot}45 < \hat{\sigma} < -0{\cdot}35$, in which a periodic solution undergoes a period doubling sequence of bifurcations leading to aperiodic (likely chaotic) solutions.

Figure 4 provides phase planes and frequency decompositions of A_{1N} at a representative values of $\hat{\sigma}$ in each of the first four period-doubled regions of Figure 3, with a final phase plane and frequency decomposition of A_{1N} at a value of $\hat{\sigma}$ corresponding to aperiodic flow. The period doubling progression is clearly illustrated as a doubling of the trajectories in the

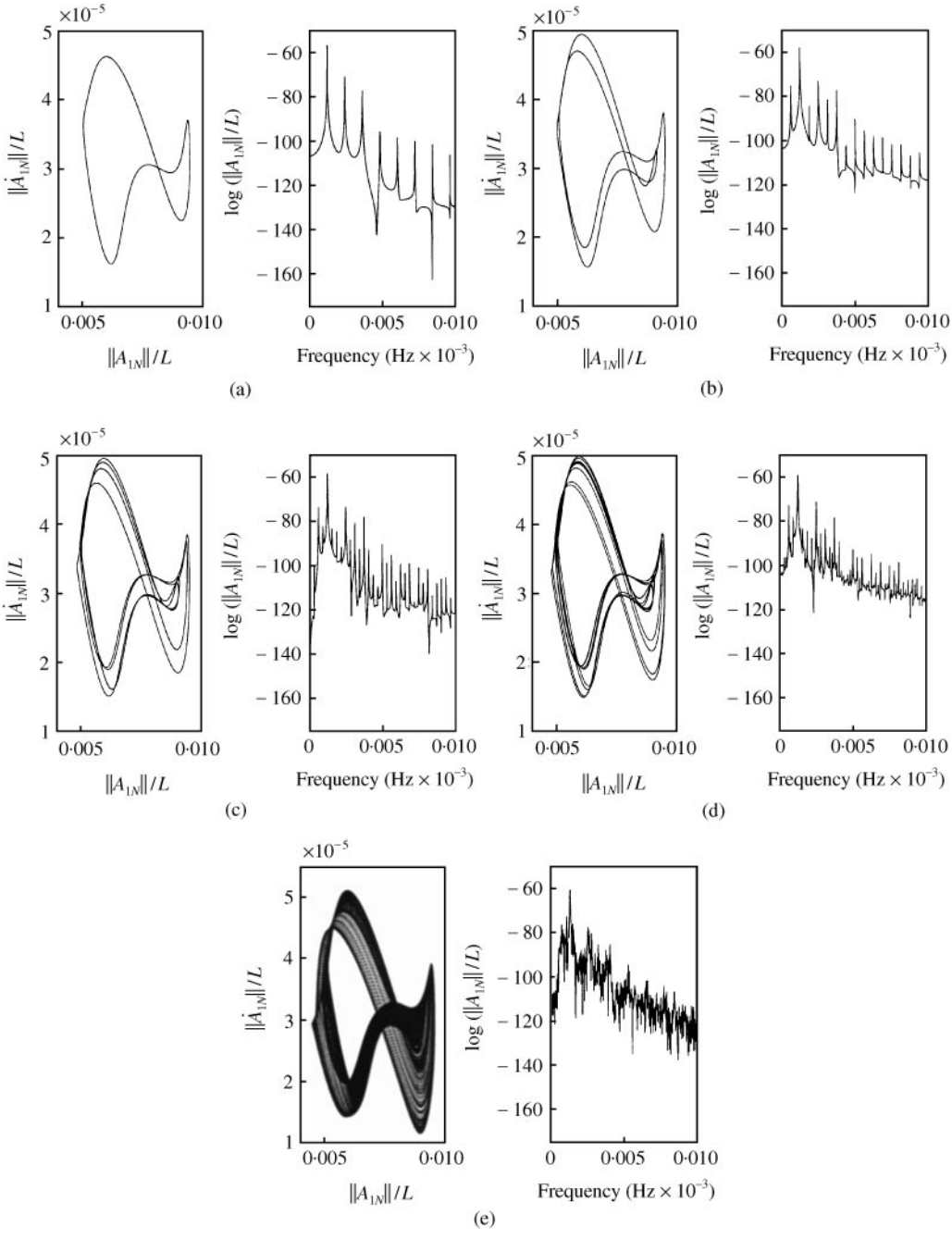

Figure 4. Phase planes representing $\|\dot{A}_{1N}\|/L$ versus $\|A_{1N}\|/L$ and corresponding power spectrum of $\|A_{1N}\|/L$ for the $a_2 = a_3 = 0$ system (defined in the caption of Figure 2) for detuning values (a) $\hat{\sigma} = 0{\cdot}45$, (b) $\hat{\sigma} = 0{\cdot}40$, (c) $\hat{\sigma} = 0{\cdot}385$, (d) $\hat{\sigma} = 0{\cdot}38$, and (e) $\hat{\sigma} = 0{\cdot}362$. 500 periods shown in each sub-figure.

phase planes, and as additional peaks in the frequency domain corresponding to $\frac{1}{2}$, $\frac{1}{4}$, $\frac{1}{8}$, … of the dominant initial frequency. Eventually, after an accumulation of period doublings, the flow appears aperiodic and exhibits broadband frequency content and a densely layered orbit, with no overlap after 500 periods (the resolution of the figure).

The description of the $\hat{\sigma}$-region above is further complicated by additional limit cycles and multiple solutions, which appear to be strongly dependent on the non-linear material properties. For example, the sequence of periodic and aperiodic solutions described in Figure 3 ends at approximately $\hat{\sigma} = 0{\cdot}21$, at which point a new periodic solution (not shown) emerges. This new limit cycle has a period equal to approximately half that of the previous limit cycle, and experiences two bifurcations as $\hat{\sigma}$ is increased in which the period increases by 1·5 at each occurrence, before finally transitioning into the stable Hopf ($H3$) limit cycle. Furthermore, a second stable limit cycle can be found at $\hat{\sigma} = 0{\cdot}38$, resulting in two stable limit cycles to the evolution equations in the neighborhood of $\hat{\sigma} = 0{\cdot}38$. Alternatively, simulations for the example non-linear material did not reveal limit cycles in the analogous $\hat{\sigma}$-regions, and thus the number and variety of periodic and aperiodic solutions can be expected to be highly dependent on the non-linear material properties.

6. CLOSING REMARKS

In this study, internal resonance mechanisms between near-commensurate longitudinal and transverse modes of a taut spatial string have been identified. In particular, the example of a cubically induced internal resonance between the first longitudinal mode and the third transverse mode of an example string has been explored in detail. The example illustrates that large longitudinal motions can occur in the proximity of a transverse resonance when commensurability is approached. These motions arise as periodic, quasi-periodic, and aperiodic (likely chaotic) response to harmonic forcing.

New branches of periodic response have been identified which include in-plane transverse motions coupled to longitudinal motions, and whirling motions coupled to longitudinal motions. The existence of these new branches acts as a destabilizing effect on the previously documented, longitudinally non-resonant, in-plane and whirling solutions. The stability of the new branches, as well as their softening–hardening nature, has been shown to be dependent on the non-linear material characterization.

Complex dynamics have been documented in regions of detuning in which no stable periodic solutions exist. In particular, stable quasi-periodic response and period doubling tori (corresponding to periodic response and period doubling sequences in the evolution equations) have been identified, with the latter culminating in densely layered orbits in the state space and aperiodic, likely chaotic, response.

ACKNOWLEDGMENTS

This research is supported in part by the Israel Science Foundation founded by the Israel Academy of Sciences under grant no. 20697. O. G. thanks the Fund for Promotion of Research at the Technion and M. J. L. thanks the Koret Foundation for their postdoctoral award.

REFERENCES

1. R. NARASIMHA 1968 *Journal of Sound and Vibration* **8**, 134–146. Non-linear vibration of an elastic string.
2. J. MILES 1984 *Journal of the Acoustical Society of America* **75**, 1505–1510. Resonant, nonplanar motion of a stretched string.
3. J. M. JOHNSON and A. K. BAJAJ 1989 *Journal of Sound and Vibration* **128**, 87–107. Amplitude modulated and chaotic dynamics in resonant motion of strings.

4. T. C. A. MOLTENO and N. B. TUFILLARO 1990 *Journal of Sound and Vibration* **137**, 327–330. Torus doubling and chaotic string vibrations: experimental results.
5. O. O'REILLY and P. J. HOLMES 1992 *Journal of Sound and Vibration* **153**, 413–435. Non-linear, non-planar, non-periodic vibrations of a string.
6. A. K. BAJAJ and J. M. JOHNSON 1992 *Philosophical Transactions of the Royal Society of London* **338**, 1–41. On the amplitude dynamics and crisis in resonant motions of stretched strings.
7. O. O'REILLY 1993 *International Journal of Non-Linear Mechanics* **28**, 337–351. Global bifurcations in the forced vibration of a damped string.
8. M. B. RUBIN and O. GOTTLIEB 1996 *Journal of Sound and Vibration* **197**, 85–101. Numerical solutions of forced vibration and whirling of a non-linear string using the theory of a cosserat point.
9. C. LEE and N. C. PERKINS 1992 *Nonlinear Dynamics* **3**, 465–490. Nonlinear oscillations of suspended cables containing a two-to-one internal resonance.
10. S. A. NAYFEH, A. H. NAYFEH and D. T. MOOK 1995 *ASME Journal of Vibration and Control* **1**, 307–334. Nonlinear response of a taut string to longitudinal and transverse end excitation.
11. M. J. LEAMY and O. GOTTLIEB 1999 *1999 ASME Design Engineering Technical Conferences*, *Las Vegas*, *U.S.A.*, DETC-99/VIB-8155. Nonlinear dynamics of a taut spatial string with material nonlinearities.
12. J. T. ODEN 1972 *Finite Elements of Nonlinear Continua*. New York: McGraw-Hill.
13. L. MEIROVITCH 1997 *Principles and Techniques of Vibrations*. London: Prentice-Hall.
14. A. LUONGO and A. PAOLONE 1999 *Nonlinear Dynamics*. On the reconstitution problem in the multiple time scale method (to appear).
15. E. J. DOEDEL and X. J. WANG 1995 *Technical Report CRPC*-95-2, *Center for Research on Parallel Computing*, *California Institute of Technology*, *Pasadena*, *CA*. AUTO94. Software for continuation and bifurcation problems on ordinary differential equations.
16. T. S. PARKER and L. O. CHUA 1989 *Practical Numerical Algorithms for Chaotic Systems*. New York: Springer-Verlag.

APPENDIX A: $O(\varepsilon^2)$ GOVERNING EQUATIONS

The $O(\varepsilon^2)$ governing equations are

$$
\begin{aligned}
&j^2r^2\omega_t^2D_0^2u_2 - r^2\omega_t^2\frac{\partial^2u_2}{\partial x^2}\\
&\quad = -\left[j^2r^2\omega_t^2(2D_0D_2 + D_1^2) + \sigma_2D_0^2 + c_{11}D_1\right.\\
&\qquad \left. + c_{12}D_0 + 2(\sigma_1 + j^2\sigma_r\omega_t^2)D_0D_1\right]u_0\\
&\qquad - \left[(\sigma_1 + j^2\sigma_r\omega_t^2)D_0^2 + c_{11}D_0 + 2j^2r^2\omega_t^2D_0D_1\right]u_1\\
&\qquad + D_0\left[C_1\left(\frac{\partial v_0}{\partial x}\frac{\partial^2v_0}{\partial x^2} + \frac{\partial w_0}{\partial x}\frac{\partial^2w_0}{\partial x^2} + \frac{\partial^2u_1}{\partial x^2}\right) + C_2\frac{\partial^2u_0}{\partial x^2}\right] + D_1\left[C_1\frac{\partial^2u_0}{\partial x^2}\right]\\
&\qquad + a_2\omega_t^2(r^2-1)\left[2\frac{\partial u_1}{\partial x}\frac{\partial^2u_0}{\partial x^2} + 2\frac{\partial u_0}{\partial x}\frac{\partial^2u_1}{\partial x^2} + \frac{2\sigma_r}{r^2-1}\frac{\partial^2u_0}{\partial x^2}\frac{\partial u_0}{\partial x}\right.\\
&\qquad + 3\left(\frac{\partial u_0}{\partial x}\right)^2\frac{\partial^2u_0}{\partial x^2} + \frac{\partial^2u_0}{\partial x^2}\left(\left(\frac{\partial v_0}{\partial x}\right)^2 + \left(\frac{\partial w_0}{\partial x}\right)^2\right)\\
&\qquad \left. + 2\frac{\partial u_0}{\partial x}\left(\frac{\partial v_0}{\partial x}\frac{\partial^2v_0}{\partial x^2} + \frac{\partial w_0}{\partial x}\frac{\partial^2w_0}{\partial x^2}\right)\right] + 3a_3\omega_t^2(r^2-1)\left(\frac{\partial u_0}{\partial x}\right)^2\frac{\partial^2u_0}{\partial x^2}
\end{aligned}
$$

$$+\omega_t^2(r^2-1)\left[2\frac{\partial u_0}{\partial x}\frac{\partial^2 u_1}{\partial x^2}+2\frac{\partial u_1}{\partial x}\frac{\partial^2 u_0}{\partial x^2}+\frac{\partial v_0}{\partial x}\frac{\partial^2 v_1}{\partial x^2}+\frac{\partial v_1}{\partial x}\frac{\partial^2 v_0}{\partial x^2}\right.$$

$$\left.+\frac{\partial w_0}{\partial x}\frac{\partial^2 w_1}{\partial x^2}+\frac{\partial w_1}{\partial x}\frac{\partial^2 w_0}{\partial x^2}\right]$$

$$+\sigma_r\omega_t^2\left[\frac{\partial^2 u_1}{\partial x^2}+2\frac{\partial^2 u_0}{\partial x^2}\frac{\partial u_0}{\partial x}+\frac{\partial^2 v_0}{\partial x^2}\frac{\partial v_0}{\partial x}+\frac{\partial^2 w_0}{\partial x^2}\frac{\partial w_0}{\partial x}\right], \tag{A.1}$$

$$j^2r^2\omega_t^2D_0^2v_2-\omega_t^2\frac{\partial^2 v_2}{\partial x^2}=-\left[j^2r^2\omega_t^2(2D_0D_2+D_1^2)+\sigma_2D_0^2+c_{21}D_1\right.$$

$$\left.+c_{22}D_0+2(\sigma_1+j^2\sigma_r\omega_t^2)D_0D_1\right]v_0$$

$$-\left[(\sigma_1+j^2\sigma_r\omega_t^2)D_0^2+c_{21}D_0+2j^2r^2\omega_t^2D_0D_1\right]v_1$$

$$+D_0\left[C_1\left(\frac{\partial^2 v_0}{\partial x^2}\frac{\partial u_0}{\partial x}+\frac{\partial v_0}{\partial x}\frac{\partial^2 u_0}{\partial x^2}\right)\right]$$

$$+a_2\omega_t^2(r^2-1)\left[\frac{\partial^2 v_0}{\partial x^2}\left(\frac{\partial u_0}{\partial x}\right)^2+2\frac{\partial v_0}{\partial x}\frac{\partial u_0}{\partial x}\frac{\partial^2 u_0}{\partial x^2}\right]$$

$$+\omega_t^2(r^2-1)\left[\frac{\partial^2 v_0}{\partial x^2}\left(\frac{\partial u_1}{\partial x}+\frac{3}{2}\left(\frac{\partial v_0}{\partial x}\right)^2\right.\right.$$

$$\left.\left.+\frac{1}{2}\left(\frac{\partial w_0}{\partial x}\right)^2\right)+\frac{\partial v_0}{\partial x}\left(\frac{\partial^2 u_1}{\partial x^2}+\frac{\partial w_0}{\partial x}\frac{\partial^2 w_0}{\partial x^2}\right)+\frac{\partial v_1}{\partial x}\frac{\partial^2 u_0}{\partial x^2}+\frac{\partial^2 v_1}{\partial x^2}\frac{\partial u_0}{\partial x}\right]$$

$$+\sigma_r\omega_t^2\left[\frac{\partial^2 v_0}{\partial x^2}\frac{\partial u_0}{\partial x}+\frac{\partial v_0}{\partial x}\frac{\partial^2 u_0}{\partial x^2}\right], \tag{A.2}$$

$$j^2r^2\omega_t^2D_0^2w_2-\omega_t^2\frac{\partial^2 w_2}{\partial x^2}=-\left[j^2r^2\omega_t^2(2D_0D_2+D_1^2)+\sigma_2D_0^2+c_{31}D_1\right.$$

$$\left.+c_{32}D_0+2(\sigma_1+j^2\sigma_r\omega_t^2)D_0D_1\right]w_0$$

$$-\left[(\sigma_1+j^2\sigma_r\omega_t^2)D_0^2+c_{31}D_0+2j^2r^2\omega_t^2D_0D_1\right]w_1$$

$$+D_0\left[C_1\left(\frac{\partial^2 w_0}{\partial x^2}\frac{\partial u_0}{\partial x}+\frac{\partial w_0}{\partial x}\frac{\partial^2 u_0}{\partial x^2}\right)\right]+a_2\omega_t^2(r^2-1)\left[\frac{\partial^2 w_0}{\partial x^2}\left(\frac{\partial u_0}{\partial x}\right)^2\right.$$

$$\left.+2\frac{\partial w_0}{\partial x}\frac{\partial u_0}{\partial x}\frac{\partial^2 u_0}{\partial x^2}\right]+\omega_t^2(r^2-1)\left[\frac{\partial^2 w_0}{\partial x^2}\left(\frac{\partial u_1}{\partial x}+\frac{1}{2}\left(\frac{\partial v_0}{\partial x}\right)^2\right.\right.$$

$$\left.\left.+\frac{3}{2}\left(\frac{\partial w_0}{\partial x}\right)^2\right)+\frac{\partial w_0}{\partial x}\left(\frac{\partial^2 u_1}{\partial x^2}+\frac{\partial v_0}{\partial x}\frac{\partial^2 v_0}{\partial x^2}\right)+\frac{\partial w_1}{\partial x}\frac{\partial^2 u_0}{\partial x^2}+\frac{\partial^2 w_1}{\partial x^2}\frac{\partial u_0}{\partial x}\right]$$

$$+\sigma_r\omega_t^2\left[\frac{\partial^2 w_0}{\partial x^2}\frac{\partial u_0}{\partial x}+\frac{\partial w_0}{\partial x}\frac{\partial^2 u_0}{\partial x^2}\right]. \tag{A.3}$$

APPENDIX B. PROCEDURE OF DETERMINING AUTONOMOUS EVOLUTION EQUATIONS

This appendix provides the procedure for determining the autonomous evolution equations from the $O(\varepsilon^1)$ and $O(\varepsilon^2)$ solvability conditions.

The $O(\varepsilon^2)$ solvability conditions are determined to be

$$
\begin{aligned}
&-[2(rN)^2\pi^2\omega_t^2 \mathrm{i}D_2 - \sigma_2 + \mathrm{i}(c_{12} + (N\pi)^2 C_2)]A_{1N} \\
&\quad + \frac{(r^2-1)\pi^4 N^4 \omega_t^2}{4r^2}[4(r^2-1)(a_2+1)^2 - 9(a_2+a_3)r^2]A_{1N}|A_{1N}|^2 \\
&\quad + \frac{(r^2-1)\pi^4 N^4 r^2 \omega_t^2}{2}[r^2 - a_2 - 1]\bar{A}_{1N}(A_{2rN}^2 + A_{3rN}^2) \\
&\quad + \frac{(r^2-1)\pi^4 N^4 r^2 \omega_t^2}{9r^2-1}[3r^4 - (9a_2+8)r^2 + a_2 + 1]A_{1N}(|A_{2rN}|^2 + |A_{3rN}|^2) \\
&\quad = 0, \qquad \text{(B.1)} \\
&-[2(rN)^2\pi^2\omega_t^2 \mathrm{i}D_2 - \sigma_2 + \mathrm{i}c_{22}]A_{2rN} \\
&\quad - \frac{(r^2-1)\pi^4 N^4 r^2 \omega_t^2}{8}[(7r^2+2)A_{2rN}|A_{2rN}|^2 + (4r^2+2)A_{2rN}|A_{3rN}|^2 \\
&\quad + 3r^2 \bar{A}_{2rN} A_{3rN}^2] + \frac{(r^2-1)\pi^4 N^4 r^2 \omega_t^2}{2}[r^2 - a_2 - 1]\bar{A}_{2rN} A_{1N}^2 \\
&\quad + \frac{(r^2-1)\pi^4 N^4 r^2 \omega_t^2}{9r^2-1}[3r^4 - (9a_2+8)r^2 + a_2 + 1]A_{2rN}|A_{1N}|^2 \\
&\quad = 0, \qquad \text{(B.2)} \\
&-[2(rN)^2\pi^2\omega_t^2 \mathrm{i}D_2 - \sigma_2 + \mathrm{i}c_{32}]A_{3rN} \\
&\quad - \frac{(r^2-1)\pi^4 N^4 r^2 \omega_t^2}{8}[(7r^2+2)A_{3rN}|A_{3rN}|^2 + (4r^2+2)A_{3rN}|A_{2rN}|^2 \\
&\quad + 3r^2 \bar{A}_{3rN} A_{2rN}^2] + \frac{(r^2-1)\pi^4 N^4 r^2 \omega_t^2}{2}[r^2 - a_2 - 1]\bar{A}_{3rN} A_{1N}^2 \\
&\quad + \frac{(r^2-1)\pi^4 N^4 r^2 \omega_t^2}{9r^2-1}[3r^4 - (9a_2+8)r^2 + a_2 + 1]A_{3rN}|A_{1N}|^2 \\
&\quad = 0. \qquad \text{(B.3)}
\end{aligned}
$$

The quantities A_{1N}, A_{2rN}, A_{3rN}, p, c_i, C, t in equations (B.1)–(B.3) are dimensionless quantities which were previously denoted with a $*$. Here, we return to this notation and

TABLE B1

Description of branches appearing in Figure 2

Branch	Description	Modal content
*B*1	Simple planar	$A_{1N} = A_{3rN} = 0,\ A_{2rN} \neq 0$
*B*2	Simple whirling	$A_{1N} = 0,\ A_{2rN} \neq 0,\ A_{3rN} \neq 0$
*B*3	Composite planar	$A_{1N} \neq 0,\ A_{2rN} \neq 0,\ A_{3rN} \neq 0$
*B*4	Composite whirling	$A_{1N} \neq 0,\ A_{2rN} \neq 0,\ A_{3rN} \neq 0$

perform a reconstitution step,

$$\frac{\mathrm{d}A_{ij}^*}{\mathrm{d}t^*} = \varepsilon D_1 A_{ij}^* + \varepsilon^2 D_2 A_{ij}^*, \tag{B.4}$$

where the dimensionless quantities are related to dimensional quantities through the relationships

$$A_{ij} = \varepsilon L A_{ij}^*, \quad \frac{\mathrm{d}}{\mathrm{d}t} = \Omega \frac{\mathrm{d}}{\mathrm{d}t^*}, \quad \varepsilon^2 p^* = \frac{p}{\rho^{\mathrm{T}} A^{\mathrm{T}} L^2}, \quad \varepsilon^2 c_1^* A_{1N}^* = \frac{\Omega c_1}{L} A_{1N}, \tag{B.5}$$

$$\varepsilon^2 C^* A_{1N}^* = \frac{\Omega C}{\rho^{\mathrm{T}} L^3} A_{1N}, \quad \varepsilon^3 A_{ij}^{*3} = \frac{A_{ij}^3}{L^3}. \tag{B.6}$$

Substitution of equations (B.5) and (B.6) into equation (B.4) yields the evolution equations (47)–(49).